Comput Geosci (2018) 22:329–346
DOI 10.1007/s10596-017-9695-3

ORIGINAL PAPER

A new insight into onset of inertial flow in porous media using network modeling with converging/diverging pores

Maziar Veyskarami[1] · Amir Hossein Hassani[1] · Mohammad Hossein Ghazanfari[1]

Received: 12 November 2016 / Accepted: 4 September 2017 / Published online: 14 September 2017

Abstract The network modeling approach is applied to provide a new insight into the onset of non-Darcy flow through porous media. The analytical solutions of one-dimensional Navier-Stokes equation in sinusoidal and conical converging/diverging throats are used to calculate the pressure drop/flow rate responses in the capillaries of the network. The analysis of flow in a single pore revealed that there are two different regions for the flow coefficient ratio as a function of the aspect ratio. It is found that the critical Reynolds number strongly depends on the pore geometrical properties including throat length, average aspect ratio, and average coordination number of the porous media, and an estimation of such properties is required to achieve more reliable predictions. New criteria for the onset of non-Darcy flow are also proposed to overcome the lack of geometrical data. Although the average aspect ratio is the main parameter which controls the inertia effects, the effect of tortuosity on the onset of non-Darcy flow increases when the coordination number of media decreases. In addition, the higher non-Darcy coefficient does not essentially accelerate the onset of inertial flow. The results of this work can help to better understand how the onset of inertial flow may be controlled/changed by the pore architecture of porous media.

Keywords Onset of inertial flow · Pore network modeling · Sinusoidal/conical throats · Critical Reynolds number · Forchheimer number · Non-darcy flow criterion

✉ Maziar Veyskarami
Veyskarami.put@gmail.com

[1] Chemical and Petroleum Engineering Department, Sharif University of Technology, Azadi Ave, Tehran, Iran

1 Introduction

1.1 Onset of inertial flow

The relationship between flow rate and pressure drop in the porous media is controlled by flow regime [1, 2]. Although inertial effects are present in all velocity ranges, at low flow rates at which viscous forces are dominated pressure-flow rate relation is linear and Darcy's law is sufficient for modeling of the flow behavior [3, 4]. However, Darcy's law underestimates the pressure drop along porous media when velocity increases and inertia flow regime begins [3, 5, 6]. In particular, predictive models suffer from the inadequate accuracy induced by inertial effect when the velocity increases. In oil and gas reservoirs, diverging from the Darcy flow may occur, e.g., at the near wellbore conditions [7]. In order to capture the nonlinearities due to the inertia, Forchheimer [8] proposed an extended form of Darcy equation as follows:

$$-\frac{\Delta P}{L} = \frac{\mu}{K} v + \beta \rho v^2 \tag{1}$$

where ΔP represents the pressure drop along the porous media, L is the length of the medium, μ is the viscosity of the fluid passes through porous media, ρ is the density of the fluid, v is the apparent velocity of the fluid, and K and β are the permeability and non-Darcy coefficient of the porous media, respectively. It is generally accepted that the Forchheimer equation predicts the effects of inertia on laminar flow through the non-Darcy coefficient as an important inherent property of the porous media [3]. Fand et al. [9] conducted a comprehensive study on regimes of flow in porous media. They indicated six flow regimes by increasing velocity as pre-Darcy, Darcy, transition between Darcy and Forchheimer, Forchheimer, transition between

Forchheimer and turbulent, and turbulent flow. According to their study, the pre-Darcy regime occurs in extremely low Reynolds numbers and the transition between Darcy and Forchheimer regimes, weak inertia regime, can be approximated by a point due to its narrow range and difficulty in its characterization.

Chaudhary et al. [4] studied the flow behavior in porous media using converging/diverging pores and computational fluid dynamics. Their results show that inertial effects exist at all flow conditions and deviation from Darcy's law depends on the growth of these inertial effects. Chaudhary et al. [10] analyzed the impact of pore geometry on flow field in converging/diverging pores using a finite element method. They observed eddies in converging/diverging pores at laminar flow condition. Their finding indicates that growth rates of eddies by increasing the Reynolds number are different for different pore geometries and their behavior is complicated. Based on their results, change in hydraulic conductivity and the onset of non-Darcy flow in a porous medium are highly dependent on pore geometry.

Mei and Auriault [11] found that cubic equation of flow can represent weak inertia effects on flow behavior in porous media. However, Fourar et al. [12] confirmed that the Reynolds number range of weak inertia regime is very limited and, in a practical point of view, can be ignored in three-dimensional flow. Balhoff et al. [13] developed a model to predict corrections to Darcy's law in low Reynolds numbers. They concluded that the first correction to Darcy equation is cubic and terms with higher order are insignificant; however, in practice, Darcy's law can be employed with acceptable approximation and cubic term can also be ignored. Dullien [14] presented a comprehensive discussion on whether or not Eq. 1 is the correct physical model over the practical range of flow rates in porous media, and concluded that the Forchheimer equation is adequate in this manner. Some studies have also recovered the validity of the quadratic Forchheimer equation using various techniques such as Chen et al. [15], Whitaker [6], and Hassanizadeh and Gray [16]. In addition, Fourar et al. [12] mentioned that the Forchheimer equation is usually applied for predicting Darcy and non-Darcy flow regimes as well as their transition [12]. We also utilized the Forchheimer equation for analysis of flow behavior passing through porous media. Balhoff and Wheeler [17] mentioned that the permeability in Eq. 1 is not the intrinsic permeability of the porous media, and even Fourar et al. [12] suggested calling it Forchheimer's permeability to emphasize the difference between Darcy's and Forchheimer's permeability. On the other hand, Balhoff and Wheeler [17] mentioned that the difference between the intrinsic (obtained from Darcy's law) and Forchheimer's permeability is negligible for practical purposes. The permeability utilized in analysis presented in this study is Forchheimer's permeability.

According to the significance of non-Darcy behavior, many studies are conducted to consider its influence on description of the fluid flow through porous media which makes the numerical simulations so costly and reduces the precision [18]. This means that the presence of a suitable criterion for predicting the onset of non-Darcy effect seems necessary. Plenty of experimental and theoretical efforts have been made in order to acquire the upper limit of Darcy's law. This is usually obtained by allotting a critical Reynolds number to that limit, beyond which Darcy's law could not provide reliable results.

Chilton and Colburn [19] defined the Reynolds number as $Re = \rho D_p v / \mu$, where D_p is the diameter of packed particles in porous media and obtained the critical Reynolds number between 40 and 48 Ergun [2] re-defined this Reynolds number as $Re = \rho D_p u / \mu(1-\phi)$, where u is the velocity of fluid at pores and claimed that the critical Reynolds number was in the range of 3 to 10. In addition, through defining $Re = \rho v l / \mu$ (where l is the characteristic length of the porous medium), the critical Reynolds number was found to be 1 [20], 2 [21, 22], and 5 [22], according to their experimental observations. Green and Duwez [23] mentioned that the critical Reynolds number varied between 0.1 and 0.2 while the definition of their Reynolds number was $Re = K\beta\rho v / \mu$.

Pore network modeling coupled with its related fluid mechanics is introduced as a promising tool for investigating the various facets of transport phenomena in porous media [24–27] and macroscopic properties such as permeability, relative permeability, capillary pressure, diffusion, and non-Darcy coefficient [17, 28–32]. The network modeling approach seems to be also attractive for evaluating the upper limit of Darcy flow in porous media. Numerical modeling reported the critical Reynolds number in the range of 5 and 13 [33], and the critical Reynolds number equal to 10 was suggested by Hassanizadeh and Gray [16] using the general continuum approach adopted to thermodynamic processes in porous media. Thauvin and Mohanty [30] employed an interconnected network of spherical and cylindrical pores and obtained this critical value equal to 0.11 by defining the Reynolds number as $Re = \rho r u / \mu$ (where r is the pore throat radius). In two latter studies, the network was fixed and the sensitivity of critical Reynolds number to the pore structure was not considered. Through applying representative unit cells composed of three duct sections, Du Plessis and Masliyah [34] concluded that the critical Reynolds number ranges between 3 and 17 where $Re = \rho v d_t / \mu$ and d_t was the diameter of the throats. Ma and Ruth [35] used a periodic representative unit cell made up of the cylindrical capillaries with constant radii for modeling of the non-Darcy flow and found the critical Reynolds number between 3 and 10. However, here, an interconnected network of converging/diverging throats

with various throat profiles is applied to achieve more realistic results.

The other well-known criterion for prediction of the onset of non-Darcy flow is the critical Forchheimer number (F_{oc}). Using permeability at zero velocity (K_o) and the non-Darcy coefficient of the porous media, Ma and Ruth [35] proposed that the Forchheimer number can be defined as $F_o = K_o\beta\rho v / \mu$. Utilizing this definition, they found that the onset of nonlinearities occurs at the critical Forchheimer numbers between 0.005 and 0.02. Zeng and Grigg [36] presented the Forchheimer number regarding the critical non-Darcy effect and claimed with a 10% non-Darcy effect, the Forchheimer number would be 0.11.

Various ranges of the critical Reynolds number with different definitions lead to the difficulty for choosing an appropriate criterion for the onset of non-Darcy flow. This study tries to examine how the critical Reynolds number changes with alteration in the pore geometrical parameters of a porous medium. In other words, finding a more suitable range for the critical Reynolds number applicable to predict the onset of inertial flow in porous media with different pore structures is the main objective of this paper. Also, we specifically address this question: how a unique criterion can be introduced instead of critical Reynolds number which eliminates the dependency on geometrical properties of the pores. In what follows, the relation between Reynolds number (with various definitions) and the pore geometrical parameters including average aspect ratio, throat length, and coordination number for two kinds of throat profiles is precisely examined and new proper criteria, valid in the wide range of situations, are proposed. Due to the requirement of these criteria to the value of non-Darcy coefficient, some correlations for prediction of the non-Darcy flow coefficient and their validation are also presented.

1.2 Brief background on modeling approach

Earlier attempts for modeling of the subsurface packed beds have been done by assuming the porous medium as a bundle of tubes, such as Carman-Kozeny and Ergun equations [37]. Even though these models were successful to describe the macroscopic characteristics of porous media to some extent, they were not persuasive methods for studying the other phenomena, for instance, mixing effects. Later, in order to model the two-phase flow through compacted porous media, Fatt [38] proposed a better and more realistic approach for modeling of the porous media structure which was presented by an interconnected pore/throat network. In the first works that used Fatt's pore network modeling approach, it was assumed that the interconnections of network (nodes) were nullified, while it was evident that in the real porous media, nodes are actually the representatives of larger voids; hence, next models tried to involve the effects of nodes using innovative approaches, such as assuming separated specific elements for nodes and connected throats [30, 39].

Naturally, the porous media is of high degree of complexity from a morphological point of view [31, 37, 40, 41]. As much as a pore network model considers these structural intricacies, it would resemble the natural subsurface packed beds in a more realistic manner. On account of the converging/diverging nature of pores in the real porous media [17, 31, 42, 43], depiction of the pore space as a converging/diverging environment seems to be more realistic. As a result, in this study, the geometry of porous media is composed of an interconnected framework of sinusoidal and conical pore throats. Modeling the porous media in that manner, referred to earlier, is conducted by Balhoff and Wheeler [17]. They used an empirical correlation for calculating the pressure as a function of the flow rate in diverging/converging capillary tubes. Conversely, in this work, the pressure drop is related to the passing volumetric flow rate using the analytical solution of Navier-Stokes equation. Recently, we have discussed the role of pore space profiles on non-Darcy flow behavior in isotropic and anisotropic porous media using network modeling [44]. Here, we follow the pore network modeling procedure applied in our previous work to investigate flow behavior in Darcy and Forchheimer (non-Darcy) regimes.

Due to importance of coordination number in microscopic and macroscopic scale flow analysis in porous media, constructing networks with different coordination patterns has attracted attention in the literature [45–49]. In spite of different coordination patterns, considering cubic lattice as a bulk volume is popular in network modeling [17, 30, 31, 46] which may be because of necessity of considering a cubic form of lattice to apply boundary conditions such as periodic boundary condition to the boundary planes which are perpendicular to the flow direction. In the present work, different coordination numbers were assigned to pores of a cubic lattice by random elimination of throats to construct a network with predetermined values of the average coordination number.

In this study, a cubic lattice composed of converging/diverging throats is constructed to apply pore network modeling. The flow behavior as well as the intrinsic properties of reservoir rocks such as permeability, tortuosity, and non-Darcy coefficient are analyzed at different values of pore-scale characteristics like coordination number, aspect ratio, and throat length, to show/describe how these pore topology aspects control the permeability and non-Darcy coefficient, thus throwing light on the relative significance of these aspects on controlling the pore-scale flow behavior. New correlations for predicting the non-Darcy coefficient as a function of permeability and porosity and also other correlations for predicting tortuosity as a function of permeability/coordination number are presented.

2 Modeling

2.1 Model geometry description

Network models in the literature usually consisted of spherical pores and cylindrical pore throats as capillary tubes [31, 37, 42]. Each pore network model must fulfill the converging/diverging nature of the porous media. There are four options of pore throat profiles comprising conical, parabolic, hyperbolic, and sinusoidal. Among these profiles, conical structure is chosen because its profile does not have the curvature and sinusoidal profile structure is also selected since it can be the representative of the maximum curvature. Our network can be represented by a cubic lattice. The nodes of the lattice are representative of the pores, and the pore throats are represented by two connected half converging/diverging micro tubes. As a matter of fact, the pore bodies are not separated parts from the throats. However, we have attributed this name (pore body) to the end of throats to make a distinct difference between pores as diverging and throats as converging sections.

Figure 1 depicts the geometry of a complete converging/diverging tube with sinusoidal profile. The radius of this tube, R, as a function of the axis (x-axis) is as follows:

$$r(x) = a - b\cos(kx) \qquad -L/2 \le x \le L/2 \tag{2}$$

where

$$a = \frac{R_{\max} + R_{\min}}{2}, \quad b = \frac{R_{\max} - R_{\min}}{2}, \quad k = \frac{2\pi}{L}. \tag{3}$$

Figure 2 demonstrates the schematic of the capillary with conical profile. Likewise, for this profile, the radius (r) based on the tube length is

$$r(x) = a + b|x| \qquad -L/2 \le x \le L/2 \tag{4}$$

and

$$a = R_{\min} \quad \text{and} \quad b = \frac{2(R_{\max} - R_{\min})}{L}. \tag{5}$$

Figure 3 shows the exact structure of each pore throat in our model. The throats are consisted of two half tubes connected to each other at the middle of the throat. The random radius and length of each half section are determined using a special form of the Weibull distribution which is expressed in Eq. 6.

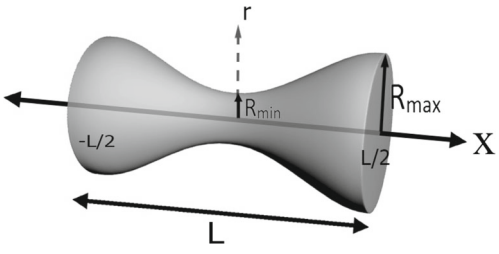

Fig. 1 Schematic of a capillary tube with sinusoidal profile [44]

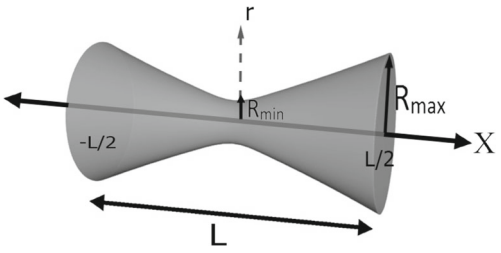

Fig. 2 Schematic of capillary tube with conical profile [44]

$$R = -\sigma(R_{i,\max} - R_{i,\min}) \times \ln\left(\text{rand} \times \left(1 - \exp\left(-\frac{1}{\sigma}\right)\right) + \exp\left(-\frac{1}{\sigma}\right)\right)^{\frac{1}{\eta}} + R_{i,\min} \tag{6}$$

where σ and η are fixed parameters. The minimum and maximum values ($R_{i,\min}$, $R_{i,\max}$) are input parameters of this function. The Weibull distribution function is applied because of its versatility, flexibility, and mathematical ease [50]. Similar functions are used by previous authors such as Diaz et al. [51] or Ioannidis and Chatzis [50]. The sum of the lengths of two half sections has a constant value which is equal to the throat length (L); the length of each half section has been calculated using Eqs. 7 and 8

$$L_1 + L_2 = L \tag{7}$$

and

$$\frac{R_1}{R_2} = \frac{L_1}{L_2}. \tag{8}$$

The section with the bigger radius at pore side has the longer length. The minimum radius of each part is equal to the throat radius generated by the Weibull distribution. Throats between the bigger bodies have larger radii. Actually, each throat between two nodes is correlated to the average size of these nodes. In this model, there is no relation that assigns pores to pores or throats to throats. In other words, two bodies with any different radius can be located near each other.

The larger radii of the six half throats which are connected to each other at each specific node are equal; it can

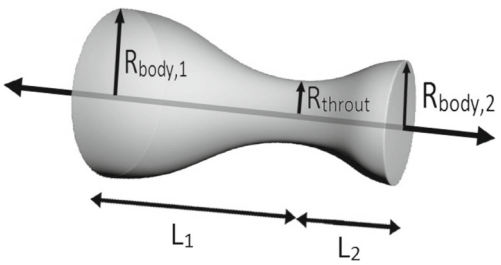

Fig. 3 Schematic of an axisymmetric capillary tube composed of two half tubes with different body radii [44]

be assumed that they are hypothetically connected to each other at the pore body. A schematic of how these half throats are connected to each other is depicted in Fig. 4a. Figure 4b illustrates a network constructed by pores with different coordination numbers.

Using Eqs. 2 and 4, the volume of each half throat can be obtained. For instance, the volume of a half sinusoidal throat can be expressed as follows:

$$V_{th} = \pi L \left(\frac{b^2}{2} + a^2 \right) \tag{9}$$

where a and b can be obtained using Eq. 3.

The summation of the volumes of all throats can be used in order to calculate the porosity of model. However, according to Fig. 4a, since the throats of lattice have overlap with each other, the volume of each pore body will be approximately calculated three times the real value and this leads to the incorrect values of porosity. So, for the calculation of the rough value of porosity, Eq. 10 is suggested and used in this study.

$$\phi = \frac{\sum V_{\text{th}} - 2 \times \sum V_b}{L_{\text{cube}}^3} \tag{10}$$

where L_{cube} is the length of the network. For simplification, hypothetic pore bodies are assumed to be spherical, and consequently, their volumes can be yielded as

$$V_{\text{b}} = \frac{4\pi r_{\text{body}}^3}{3}. \tag{11}$$

However, there may be slight inaccuracy in determination of overlapped spaces due to assuming pore body as sphere, and porosity calculated by Eq. 10 can be utilized as a representative of porosity of the network.

2.2 Flow modeling

Some of models for predicting the behavior of porous media at high velocity flow use turbulent flow correlations for bends and pipes which are not proper for that environment [17]. In reality, the flow in oil reservoirs usually remains in the laminar domain and an increase in the inertial effects causes the additional pressure drop which might be well predicted by the Forchheimer equation [30]. Although in complex systems multi-dimensional flow modeling could provide precise results, implementation of one-dimensional flow model in single capillary tubes of a network model not only provides the benefits for usage of analytical solution of Navier-Stokes equation but also gives low computational cost. Equations 12 and 13 come from the well-known Navier-Stokes equations based on the continuity and momentum balance along an axisymmetric tube in one dimension. To apply one-dimensional Navier-Stokes equation, it is assumed that the flow in capillary is axisymmetric, and also, flow profile is simplified in a lump parameter, so-called momentum correction factor; thus, dependency to θ and r directions are neglected [52–54]. In the following equations, the gravity forces are ignored [53].

$$\frac{\partial A}{\partial t} + \frac{\partial Q}{\partial x} = 0 \tag{12}$$

and

$$\frac{\partial Q}{\partial t} + \frac{\partial}{\partial x}\left(\frac{\alpha Q^2}{A} \right) + \frac{A}{\rho}\frac{\partial P}{\partial x} + \kappa \frac{Q}{A} = 0. \tag{13}$$

where A represents the cross-sectional area of the tube, P is the pressure, t is the time, Q is the volumetric flow rate ($Q = A\bar{u}$), x is the distance along the axis of the tube, α is the correction factor for axial momentum expressed by $\alpha = \int u^2 dA \,/\, A\bar{u}^2$ [53], ρ is the fluid density, μ is the viscosity of fluid, and κ is the viscosity friction coefficient which can be determined by $\kappa = 2\pi\alpha\mu \,/\, \rho(\alpha - 1)$ [52].

For steady-state conditions, the term belongs to the time in Eq. 13 becomes zero and

$$-\frac{\partial P}{\partial x} = \frac{\rho}{A}\frac{\partial}{\partial x}\left(\frac{\alpha Q^2}{A} \right) + \kappa\rho\frac{Q}{A^2} = \kappa\rho\frac{Q}{A^2} - \frac{\rho\alpha Q^2}{A^3}\frac{\partial A}{\partial x}. \tag{14}$$

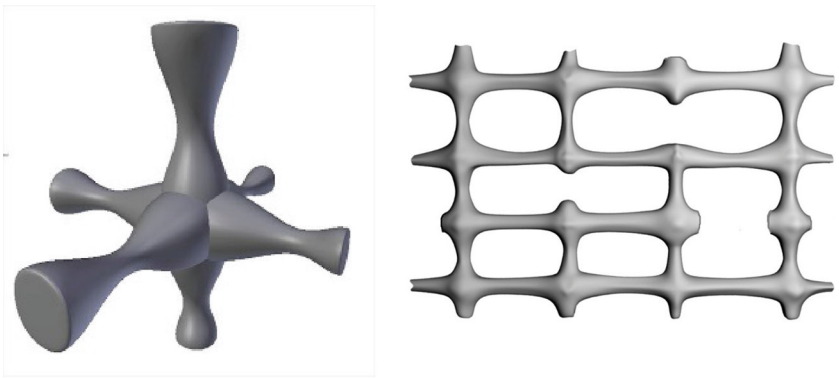

Fig. 4 **a** Connection of capillaries at pore body. **b** Two-dimensional view of a network constructed by pores with different coordination numbers [44]

The negative sign behind the left side of Eq. 14 is due to the pressure gradient in positive x direction (direction towards the axis of the tube). Equation 14 can be integrated to yield the pressure as a function of distance as follows:

$$\Delta P = \frac{\rho\alpha Q^2}{2}\left[\frac{1}{A^2}\right]_{-L/2}^{L/2} + \kappa\rho Q\int_{-L/2}^{L/2}\frac{dx}{A^2}. \tag{15}$$

For a symmetrical sinusoidal tube, the first term in the right-hand side of Eq. 15 becomes zero. According to Fig. 1, after integrating from Eq. 15, the pressure drop for symmetrical sinusoidal tube can be represented as [52]

$$\Delta P = \frac{\kappa\rho QL\left[2(R_{\max}+R_{\min})^3+3(R_{\max}-R_{\min})^2(R_{\max}+R_{\min})\right]}{16\pi^2(R_{\max}R_{\min})^{7/2}}. \tag{16}$$

Similarly, for symmetrical conical capillary [52],

$$\Delta P = \frac{\kappa\rho QL}{3\pi^2(R_{\max}-R_{\min})}\left[\frac{1}{R_{\min}^3}-\frac{1}{R_{\max}^3}\right]. \tag{17}$$

As discussed before, each throat in our network is composed of two half conical/sinusoidal tubes. Hence, the pressure drop along this geometry can be calculated by summation of the pressure drops along two parts of the each throat. Because $1/A^2$ is an even function, the pressure drop in each section equals to the half of value accounted from Eqs. 16 and 17 plus the amount of pressure drop obtained by Eqs. 18 or 19

$$P = \frac{\rho\alpha Q^2}{2}\left[\frac{1}{A^2}\right]_{0}^{L/2} \tag{18}$$

$$P = \frac{\rho\alpha Q^2}{2}\left[\frac{1}{A^2}\right]_{-L/2}^{0}. \tag{19}$$

Whether that section is diverging or converging part of the throat, Eqs. 18 or 19 should be used. For each section, the minimum radius is at the origin of tube axis. When the pressure drop is calculated in diverging part (half throat), Eq. 18 must be used; otherwise, for converging section, Eq. 19 is suitable. Since Eqs. 16 and 17 are derived using the one-dimensional Navier-Stokes equations, they include the pressure drops due to the inertial effects.

In laminar flow, the velocity profile is approximately parabolic and, due to the eddy motion, becomes flatter in turbulent flow. Since the value of α depends on the velocity profile of flowing fluid in the capillary, calculation of α which in some occasions has semi-empirical nature could be a complex and time-consuming process [55]. Thus, in this study, for the sake of simplicity, the value of $\alpha = 4/3$ is used which corresponds to the assumption of parabolic velocity profile in the capillary tubes of the network [55].

The scope of this work is based on utilizing the analytical solution of one-dimensional Navier Stokes equation in capillary tubes of the network model. In this regard, the assumptions are made, and axisymmetric flow in capillary tubes and simplified flow profile in a lump parameter, so-called momentum correction factor, are reasonable [52–54]. Analysis of flow behavior in capillary tubes based on the two- or three-dimensional geometrical model as well as variable momentum correction factor needs to numerical mesh techniques and can be in scope of future work. However, for high aspect ratio, pore application of constant momentum correction factor may be limited. Unless, the flow profile being far from turbulence which in porous media rarely flow reaches the turbulent regime [3].

The three-dimensional network is constructed using one-dimensional capillary tubes. Analytical expressions derived in these capillaries coupled with mass balance governing equations are applied for obtaining the macroscopic properties of the generated three-dimensional network models. Actually, the permeability, tortuosity, and non-Darcy coefficient are calculated by imposing different pore topology aspects like coordination number, aspect ratio, and throat length to the pores of this lattice. It should be noted that these imposed pore topology aspects do not change the one-dimensional nature of flow field in single capillaries; however, they alters the macroscopic properties of the flowing flow through network in all directions. The procedure of model implication is discussed in the next section.

It is noteworthy to mention that Eqs. 16 and 17 are also consistent for the cylindrical capillary tube. If the minimum and maximum radii of the conical or sinusoidal tube be the same ($R_{\max} = R_{\min}$), in Eqs. 16 or 17, a linear relation exists between the pressure drop and the volumetric flow rate which is known as the Hagen-Poiseuille equation.

2.3 Model implementation

At first, a certain amount of pressure drop is applied on one of the three directions of fixed lattice while periodic boundary conditions are imposed across the two other perpendicular directions of the cube. The pressure drop along each throat as a function of the flow rate can be obtained using the procedure discussed in the previous section. Then, a simple mass balance is needed to be applied at each node by

$$\sum Q_i = 0 \tag{20}$$

where Q_i is the entrance flow rate from the ith throat. Inserting the sum of Eqs. 16 to 19 in mass balance equation results in a set of nonlinear equations with unknown pressures at each node. This set of nonlinear equations can be solved using the Newton-Raphson method. First, an approximate

pressure value for each node is presumed. Then, the iteration process must be performed until the mass balance be established at all pores. Once the set of nonlinear equations has been solved, the flow rate at each throat and then the total inflow to lattice can be determined.

Rewriting Eq. 1 in the form of Eq. 21 can be used for simultaneous determination of K and β. Plotting the $\Delta P \,/(L_{\text{cube}} v\mu)$ versus $\rho v \,/\mu$ for different pressure drops leads to a straight line with a slope of β and an intercept of $1 \,/K$ (Forchheimer plot).

$$\frac{\Delta P}{L_{\text{cube}} v\mu} = \frac{1}{K} + \beta \left(\frac{\rho v}{\mu}\right). \tag{21}$$

In addition, applying this model can provide the value of dynamic tortuosity, obtained from the ratio of the streamline lengths to the straight distance. Once the flow rates at throats have been determined, a hypothetic particle can be introduced to the one of the faces of lattice. This particle can be followed in order to calculate the real path that traverses through the media. When the hypothesized particle arrives to each node, it is assumed that it moves toward the throat with the lowest restriction against the flow (i.e., the throat with the highest value of flow rate). This procedure is repeated for 15 particles that enter to the lattice from different nodes, and the final reported tortuosity is the average of the tortuosity of all particles. Also, the porosity of system can be obtained using the sum of the throat volumes and Eq. 10.

3 Results and discussion

Thauvin and Mohanty [30] claimed that the magnitude of the porous media has a negligible influence on the estimated properties of network when the size of system is larger than 14×14×14. Accordingly, the base model in this study is considered as a cube with the size of 15×15×15. The properties of the base model are listed in Table 1 which represents the minimum and maximum input of Weibull function to distribute throat and body radii (R) and the length of each throat (L_{throat}) employed to construct the lattice.

To find the more suitable distributions of pore and throat sizes, some sensitivity analysis is performed on the fixed

Table 1 Input parameters of base case used for numerical simulation

Input parameter	Value
$R_{\text{throat,min}}$ (μm)	0
$R_{\text{throat,max}}$ (μm)	6
$R_{\text{body,min}}$ (μm)	6
$R_{\text{body,max}}$ (μm)	30
L_{throat} (μm)	90
Size of system	15×15×15

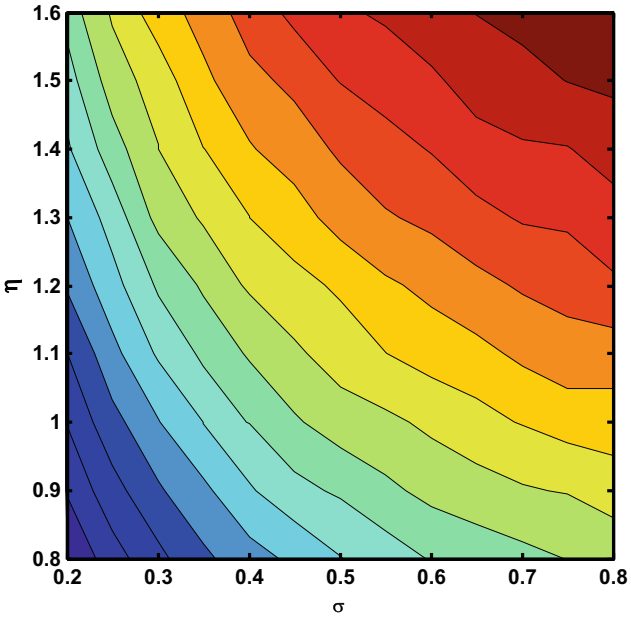

Fig. 5 Effect of parameters of Weibull function on output size distribution

parameters of Weibull distribution function, values of σ and η. σ and η were changed from 0.2 to 0.8 and from 0.8 to 1.6, respectively. The results of sensitivity analysis are shown in Fig. 5. According to this figure, an increase in the fixed parameters causes the average sizes of pores and throats tend to the maximum radius as an input parameter (the red and blue regions indicate the higher frequencies of radius size, close to the maximum and minimum input, respectively). Figure 6 shows that using $\sigma = 0.8$ and $\eta = 1.6$ gives the pore body and pore throat size distributions with highest frequencies close to the average of input parameters, i.e., maximum and minimum radii.

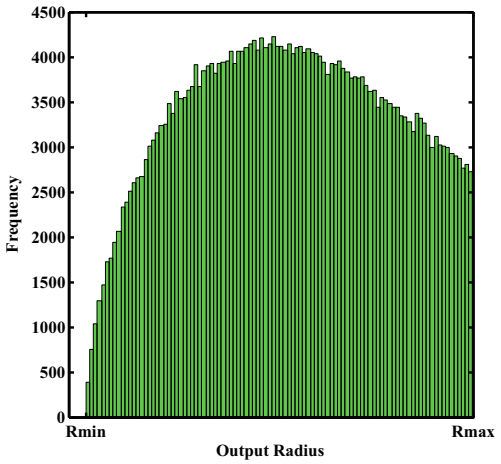

Fig. 6 Pore size distribution obtained by the Weibull distribution function with $\sigma = 0.8$ and $\eta = 1.6$

3.1 Flow parameter sensitivity analysis

3.1.1 Single pore analysis

The objective of this section is to analyze the relation between permeability and pore structure of a single pore using the Navier-Stokes analytical solution. To achieve this aim, two types of converging/diverging capillaries are considered sinusoidal and conical. The flow rate can be obtained as a function of the pressure drop by rearranging Eqs. 16 and 17. The obtained expressions for the flow rate can be inserted in Darcy's equation to calculate the flow coefficient (ψ) for a single symmetric capillary. Equations 22 and 23 represent the flow coefficients for conical and sinusoidal profiles, respectively.

$$\psi_C = K_C A_C = \frac{1.5\pi(R_{max} - R_{min})(\alpha - 1)}{\alpha\left(\frac{1}{R_{max}^3} - \frac{1}{R_{min}^3}\right)}, \tag{22}$$

$$\psi_S = K_S A_S = \frac{8\pi(R_{max}R_{min})^{3.5}(\alpha-1)}{\alpha\left(2(R_{max}+R_{min})^3+3(R_{max}-R_{min})^2(R_{max}+R_{min})\right)}, \tag{23}$$

and

$$A_C = \frac{L}{\int_{-L/2}^{+L/2} \frac{dx}{\pi(a_C+b_C|x|)^2}}, \tag{24}$$

$$A_S = \frac{L}{\int_{-L/2}^{+L/2} \frac{dx}{\pi(a_S-b_S\cos(kx))^2}}. \tag{25}$$

where

$$\int \frac{dx}{\pi\,(a_C + b_C\,|x|)^2} = -\frac{x}{\pi a_C b_C\,|x| + \pi b_C^2 x^2}, \tag{26}$$

and

$$\int \frac{dx}{\pi(a_S-b_S\cos(kx))^2} = \frac{\left(\begin{array}{l} a_S\left(b_S^2-a_S^2\right)\left(a_S\left(\tan^2\left(\frac{kx}{2}\right)+1\right)+b_S\left(\tan^2\left(\frac{kx}{2}\right)-1\right)\left(\tan^2\left(\frac{kx}{2}\right)+1\right)\right)\times\cdots \\ \left(\ln\left(\left|(b_S+a_S)\tan\left(\frac{kx}{2}\right)+\sqrt{b_S^2-a_S^2}\right|\right)-\ln\left(\left|(b_S+a_S)\tan\left(\frac{kx}{2}\right)-\sqrt{b_S^2-a_S^2}\right|\right)\right)-\cdots \\ 2b_S\left(b_S^2-a_S^2\right)^{\frac{3}{2}}\tan\left(\frac{kx}{2}\right) \end{array}\right)}{\pi\,(b_S-a_S)\left(b_S^2-a_S^2\right)^{\frac{3}{2}}k\left((b_S+a_S)\tan\left(\frac{kx}{2}\right)-\sqrt{b_S^2-a_S^2}\right)\left((b_S+a_S)\tan\left(\frac{kx}{2}\right)+\sqrt{b_S^2-a_S^2}\right)}. \tag{27}$$

Since the values of A_C and A_S for the same length of conical and sinusoidal capillaries are approximately equal, the ratio of ψ_S to ψ_C is the representative of $K_S\,/K_C$.

Figure 7 demonstrates the relation between the $\psi_S\,/\psi_C$ and $R_{max}\,/R_{min}$ (throat aspect ratio). The R_{max} is constantly kept at the value of 30 µm while the R_{min} changes in the range of 0.1 and 30 µm. By converging the $R_{max}\,/R_{min}$ to 1, the capillaries gain the shape of a cylinder, and consequently, their flow coefficient will be equal. In general, an increase in the $R_{max}\,/R_{min}$ causes a decrease in the $\psi_S\,/\psi_C$ which means when the difference between the R_{max} and R_{min} increases, the permeability of sinusoidal capillary shows more reduction than conical. As can be seen in this plot, in region A, the rate of reduction in the $\psi_S\,/\psi_C$ is much more than that in region B. In region A, the $R_{max}\,/R_{min}$ changes in the range of 1 to 30 and the dominant parameter affecting the $\psi_S\,/\psi_C$ is the curvature of tubes. The alteration of curvature for the sinusoidal duct is more drastic than the conical which reduces the sinusoidal flow coefficient. On the contrary, in region B, the R_{min} plays an more important role in variation of $\psi_S\,/\psi_C$ and this is true for both types of the capillaries which results in this fact that an increase in the $R_{max}\,/R_{min}$ cannot remarkably alter the $\psi_S\,/\psi_C$.

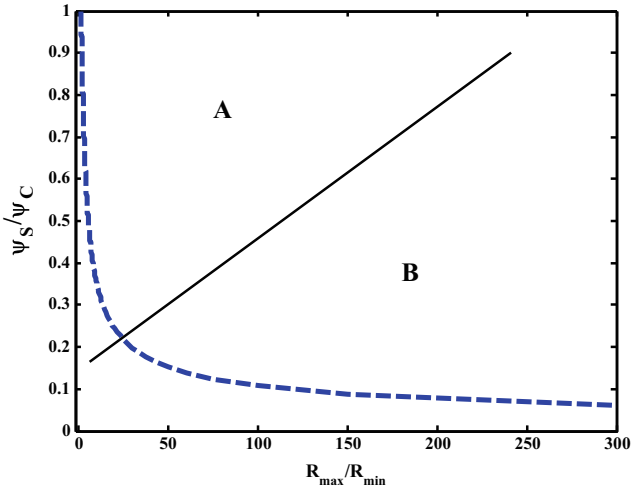

Fig. 7 Effect of throat aspect ratio on the sinusoidal-conical flow coefficient ratio

3.1.2 Network-scale analysis

Pore-scale morphology has significant effects on the macroscopic properties of porous media. In order to study the flow properties of porous media, necessary inputs of the pore space characterizing are pore body size, pore throat size, and pore coordination number [50]. Here, the average aspect ratio is defined as the average of body to throat radius ratios (R_b / R_t). The length of throat (L) is another effective parameter on the geometry of pore space.

As shown in Fig. 8, once the throat length decreases, the permeability rises. Reduction in the length of throats results in the increasing of pore profile curvature which automatically raises the restriction against the flow, but it also reduces the friction. On the other hand, increasing throat length of the network decreases the ratio of normal to flow area which allows passing of fluid in microscopic scale to the area which is considered in macroscopic flow equations.

Figure 9 illustrates the permeability alteration versus the average coordination number of the system for two types of networks, composed of the sinusoidal and conical capillaries, respectively. It can be found that the more average coordination number results in the more permeability. With a decrease in the average coordination number, the fluid should flow through the tortuous path; so, the permeability of porous media decreases. Based on the results, the conical network is a bit more sensitive to the average coordination number.

Because of the considerable effect of average aspect ratio on the permeability, the analysis is conducted in two ranges. According to Fig. 10, at low ranges of the average aspect ratio (1 to 2.6), an increase in the average aspect ratio causes a decrease in permeability, an increase in the non-Darcy coefficient, and an additional difference between the values of permeability and non-Darcy coefficient for the conical and sinusoidal network models. Continuing in the increase of average aspect ratio (which is observable in Fig. 11) results in the convergence of permeability of two networks; on the contrary, for the non-Darcy coefficient, a diverging trend continues which shows that the aspect ratio is the dominant parameter on the non-Darcy coefficient. By changing the shape of capillaries from cylindrical to conical and sinusoidal, the difference between the permeability values of two networks increases. This is because of the restriction induced by various curvatures. At high values of the average aspect ratio, the radius of throats becomes the controlling parameter. As the value of throat radius is the same for two systems, the permeability of them is close to each other.

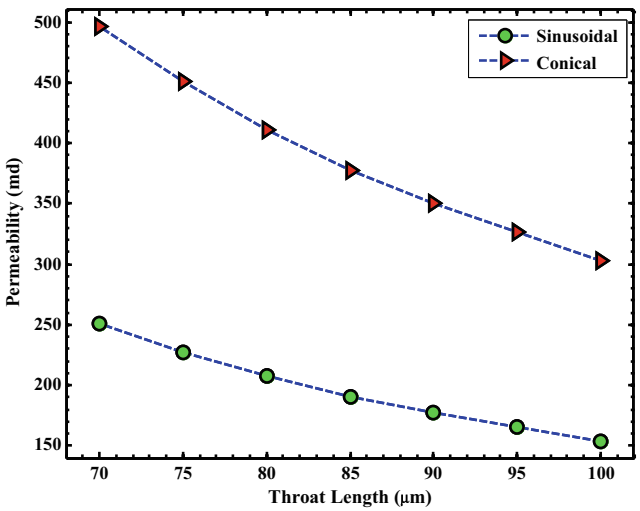

Fig. 8 Effect of throat length on the permeability of the system. The average aspect ratio and the average coordination number are 5.9 and 6, respectively

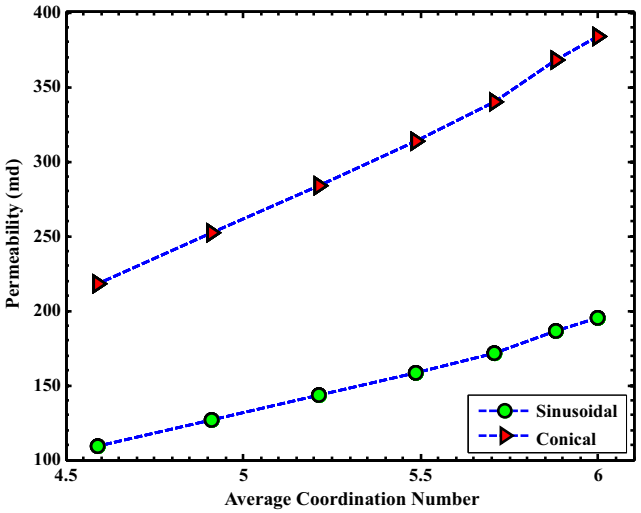

Fig. 9 Effect of average coordination number on the permeability of the sinusoidal and conical networks. The average aspect ratio and the throat length are 5.9 and 90 μm, respectively

Figures 12 and 13 contain information about the permeability and non-Darcy coefficient values based on the different lengths, average aspect ratios, and average coordination numbers. For alteration of the aspect ratio, it is possible to change the average of pore body radii while the average of pore throat sizes is constant or change the average throat size once the average of pore body radii being kept constant. Both of these scenarios are applied to the model; however, it was found that just alteration of the average throat size can remarkably affect the permeability of network. Accordingly, here, just the results of simulation by changing the average of pore throat radii are shown. Aspect ratio is a controlling parameter of the pore space curvature when a particular type of capillary is used to construct the network. The increase of aspect ratio brings about the increase of curvature and inertial effects and more resistance against the flow in a particular capillary geometry.

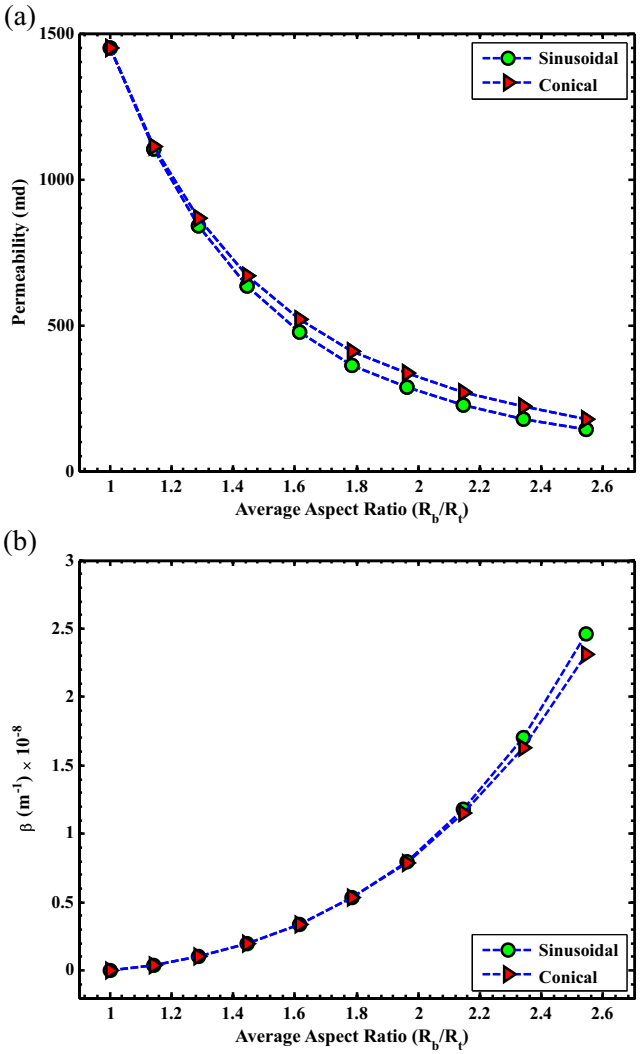

Fig. 10 Dependency of **a** permeability and **b** non-Darcy coefficient on the average aspect ratio at low ranges. The average coordination number and the throat length are 6 and 90 µm. respectively

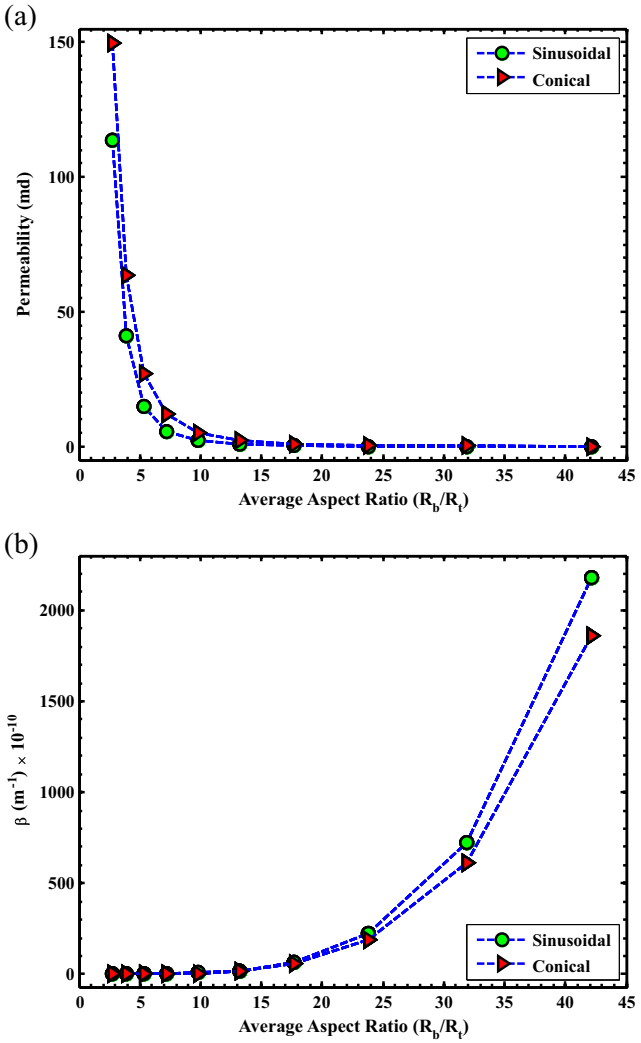

Fig. 11 Dependency of **a** permeability and **b** non-Darcy coefficient on the average aspect ratio at high ranges. The average coordination number and the throat length are 6 and 90 μm, respectively

Also, the aspect ratio directly affects the amount of friction at pore throat section. As a result, it seems reasonable that the aspect ratio be more effective on the permeability and non-Darcy coefficient than the throat length or the coordination number. The permeability and non-Darcy coefficient also show more sensitivity to alteration of the average aspect ratio at higher values than lower values. Meanwhile, the effect of change in the average aspect ratio on the alteration of permeability and non-Darcy coefficient of sinusoidal network is more than the conical one.

3.2 Non-Darcy flow onset

The more the velocity of fluid, the more the effect of inertia. The pressure drop along the porous media versus the volumetric flow rate for different aspect ratios and coordination numbers is shown in Fig. 14. As can be seen, increasing average aspect ratio and decreasing average coordination number result in an increase of pressure drop along porous media and decrease the value of flow rate at which non-Darcy flow begins. Even at low flow rates, the inertial effects exist; however, at a specific flow rate, the inertial pressure drop becomes dominant. It is assumed that this specific flow rate is the flow rate at which, the pressure drop related to the inertia consists 30% of the total pressure drop. This specific flow rate is called the onset of non-Darcy flow. It is hypothesized that at flow rates lower than this onset, the inertial effects are insignificant. For the conical and sinusoidal networks of the base case, the velocities of non-Darcy onset are 0.00249 and 0.00431 m/s, respectively. The throat Reynolds number is defined as $Re_{\mathrm{T}} = 2\rho v R_{\mathrm{t}} \big/ \mu$, where R_{t} is the average throat radius. For the base case composed of conical throats, the onset happens when $Re_{\mathrm{T}} = 0.0156$, while for sinusoidal network, the onset is at $Re_{\mathrm{T}} = 0.0271$.

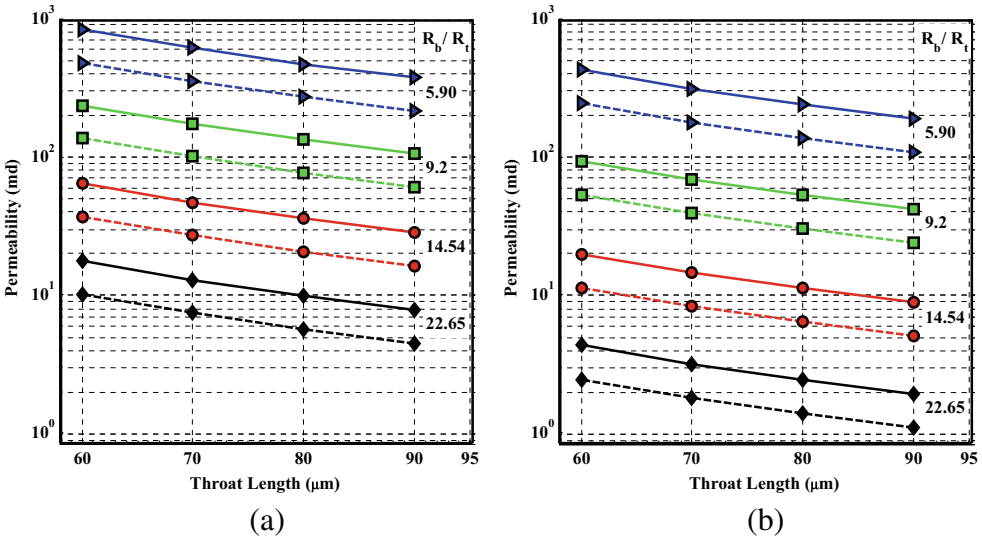

Fig. 12 Permeability relation with throat length, average aspect ratio, and average coordination number 4.5 (dash line) and 6 (solid line) for networks composed of **a** conical and **b** sinusoidal capillaries

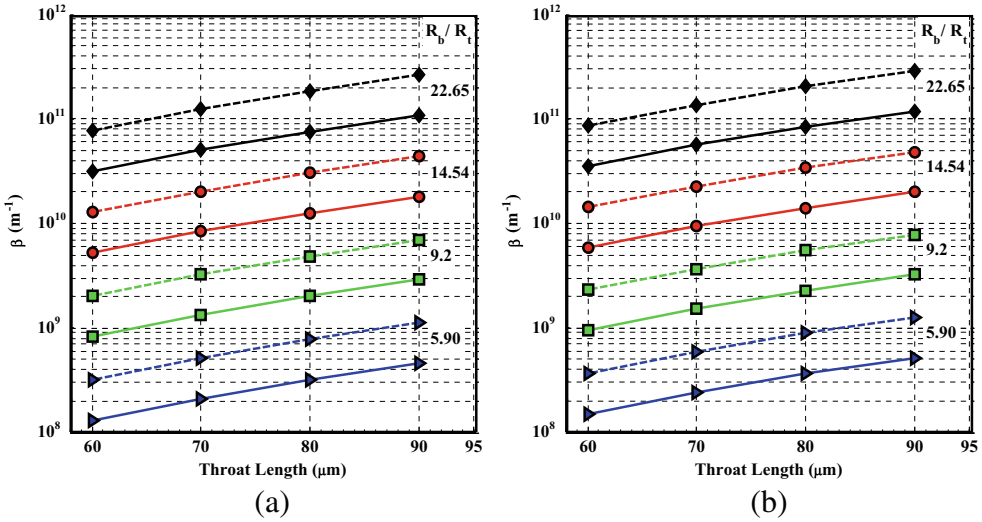

Fig. 13 Non-Darcy coefficient based on throat length, average aspect ratio, and average coordination number 4.5 (dash line) and 6 (solid line) for networks composed of **a** conical and **b** sinusoidal capillaries

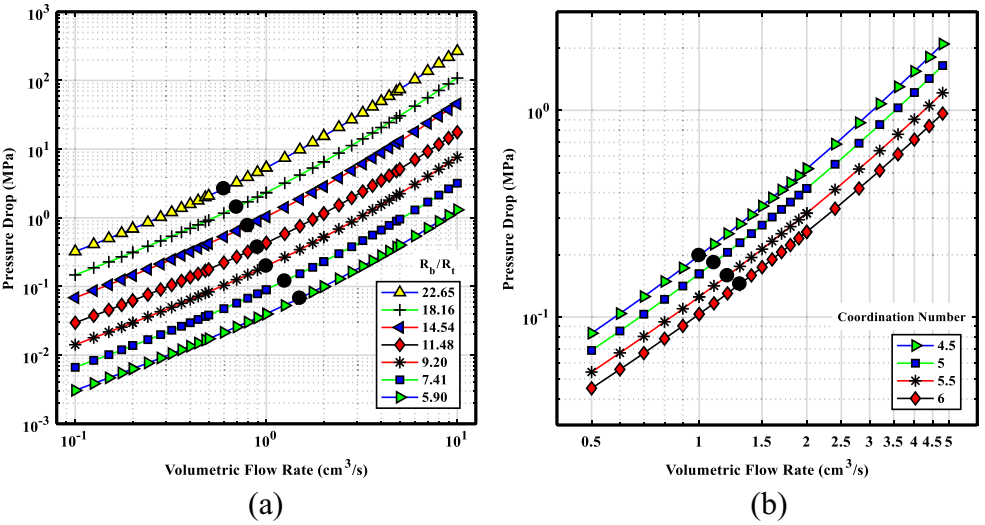

Fig. 14 Effect of **a** average aspect ratio and **b** average coordination number on pressure drop-volumetric flow rate behavior of the network. Black markers show the onset of non-Darcy flow

The onset based on the throat Reynolds number varies with the alteration of morphological properties of throats. In Fig. 15, the onset on Forchheimer regime expressed as the throat Reynolds number is shown versus the throat length, average coordination number, and average aspect ratio of the system for conical and sinusoidal networks. The effect of throat length on the onset is less than the effect of average aspect ratio alteration or average coordination number of the system. Figure 15a, b demonstrates the effect of the average aspect ratio and coordination number on the onset of non-Darcy flow based on the throat Reynolds number, respectively. A decrease in the average aspect ratio and average coordination number leads to the less value of apparent velocity required for the beginning of inertial flow. An increase in the throat length does the same. It is obvious with an increase in the value of average aspect ratio the throat Reynolds numbers, at which the onset of non-Darcy flow happens, for the sinusoidal and conical networks converge to each other. As discussed before, at high values of the average aspect ratio, pore throat radius is the controlling parameter of the permeability which causes the convergence of permeability values. On the other hand, the average aspect ratio is the dominant factor on the non-Darcy coefficient. Likewise, the convergence of non-Darcy flow onset values indicates that at high values of the aspect ratio, the main element that affects the flow behavior is pore throat radius. According to Fig. 15b, the decreasing coordination number causes the reducing of the Reynolds throat number at which the onset of non-Darcy flow occurs. This stems from that the reduction in the average coordination number leads to the increase in tortuosity of the system. Generally, it can be inferred that tortuosity considerably affects the onset of non-Darcy flow and flow behavior. Also, Figs. 16 and 17 show the critical throat Reynolds number versus the throat length and average aspect ratio for conical and sinusoidal networks with various average coordination numbers.

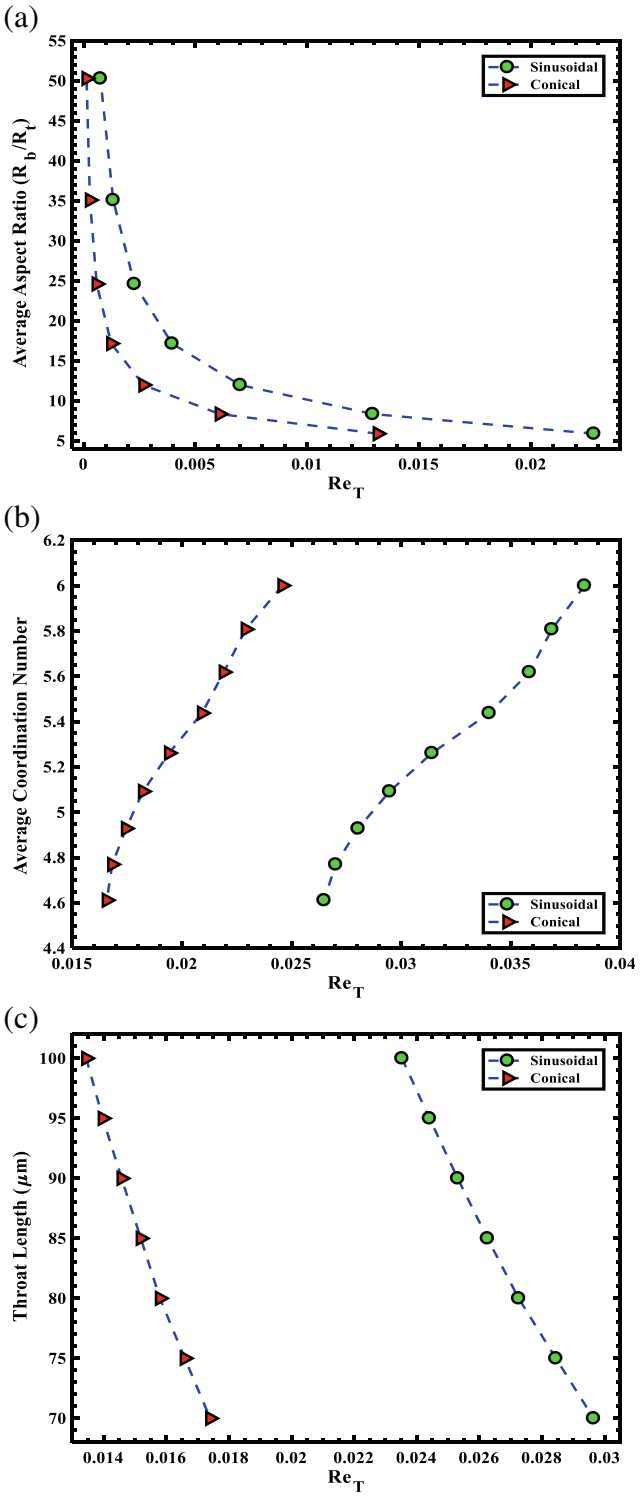

Fig. 15 Effect of **a** average aspect ratio, **b** average coordination number, and **c** throat length on the onset of non-Darcy flow for conical and sinusoidal networks

Another definition of Reynolds number is based on the characteristic length or permeability of the porous media which can be shown as $Re_K = \rho v\sqrt{K}/\mu$ and here is called permeability Reynolds number. Figures 18 and 19 present the permeability Reynolds number versus the throat length, average aspect ratio, and average coordination number for conical and sinusoidal networks. The permeability Reynolds number shows the similar behavior to the throat Reynolds number with alteration of the geometrical parameters. According to Figs. 16 to 19, it is possible to estimate the onset of inertial flow based on the pore geometrical parameters such as throat length, average aspect ratio, and average coordination number.

The other remarkable finding is that even though the permeability of conical network is more than the permeability of sinusoidal and also the non-Darcy coefficient value of conical network is higher than sinusoidal system, the non-Darcy flow onset of conical framework occurs at lower apparent velocity. It is widely accepted in the literature thatin porous media with a higher value of non-Darcy

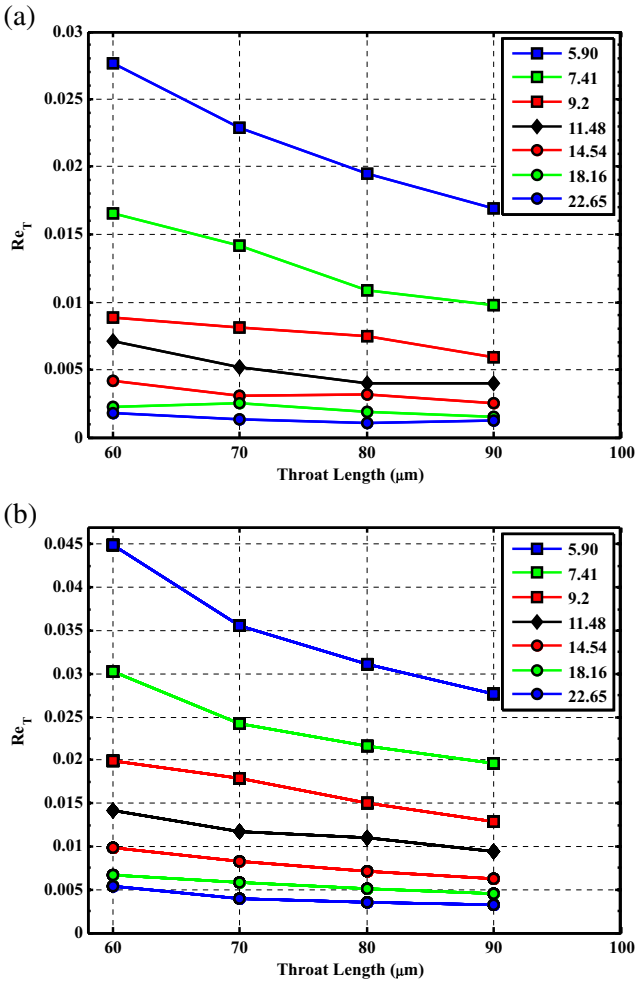

Fig. 16 Throat Reynolds number versus throat length and average aspect ratio for **a** conical and **b** sinusoidal networks with the average coordination number = 6

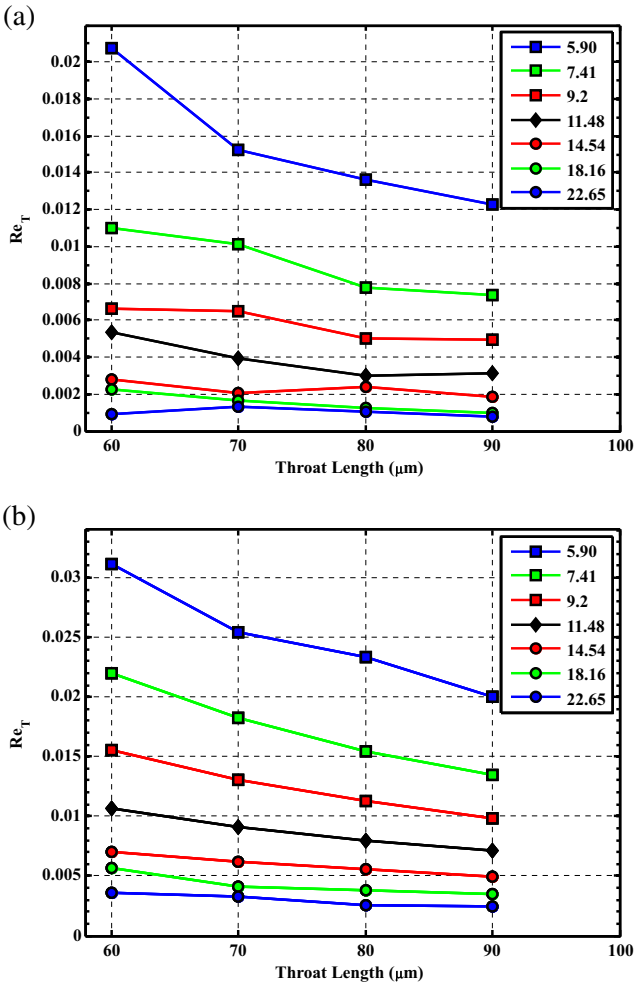

Fig. 17 Throat Reynolds number versus throat length and average aspect ratio for a) conical and b) sinusoidal networks with average coordination number=4.5

coefficient, the inertial flow begins at lower apparent velocity. Therefore, understanding the relation between permeability and non-Darcy coefficient of the porous media is a crucial parameter in the determination of the inertial flow onset. It seems that the throat Reynolds number is not a proper criterion for the prediction of non-Darcy flow onset because it just considers the throat radius while many other pore characteristics affect the onset. In addition, critical throat and permeability Reynolds numbers usually happen in a range. A good criterion should contain the macroscopic properties such as permeability, non-Darcy coefficient, or both of them which better reflects those pore characteristics and also it should be constant and valid for all conditions.

The clearly defined relation between the permeability and non-Darcy coefficient is regarded by the Forchheimer number. At higher flow rates, the inertial pressure drop increases until the Darcy flow can be ignored and flow rate becomes proportional to the square of pressure drop gradient. This can be seen in Fig. 20 which is based on the Forchheimer number ($Fo = K\beta\rho v / \mu$), where v is the apparent velocity of porous media. The Forchheimer number is the ratio of the inertial forces to the viscous forces [5]. Darcy pressure drop and non-Darcy pressure drop values are equal at the Forchheimer number equal to 1. Non-Darcy effect (E) is the ratio of the inertial pressure drop to the total pressure drop [36]. The relation between Fo and E can be represented in Eq. (28) as follows:

$$Fo = \frac{E}{1-E}. \tag{28}$$

By assuming a specific limit for the onset of non-Darcy flow, the critical Forchheimer number at which the inertial flow begins will be a constant value. For instance, here, the upper limit for Darcy flow is once the ratio of the inertial pressure drop to the total pressure drop be 30%. In this case, the critical Forchheimer number would be 0.42.

The necessity to know the value of non-Darcy coefficient is the major shortcoming of using the Forchheimer

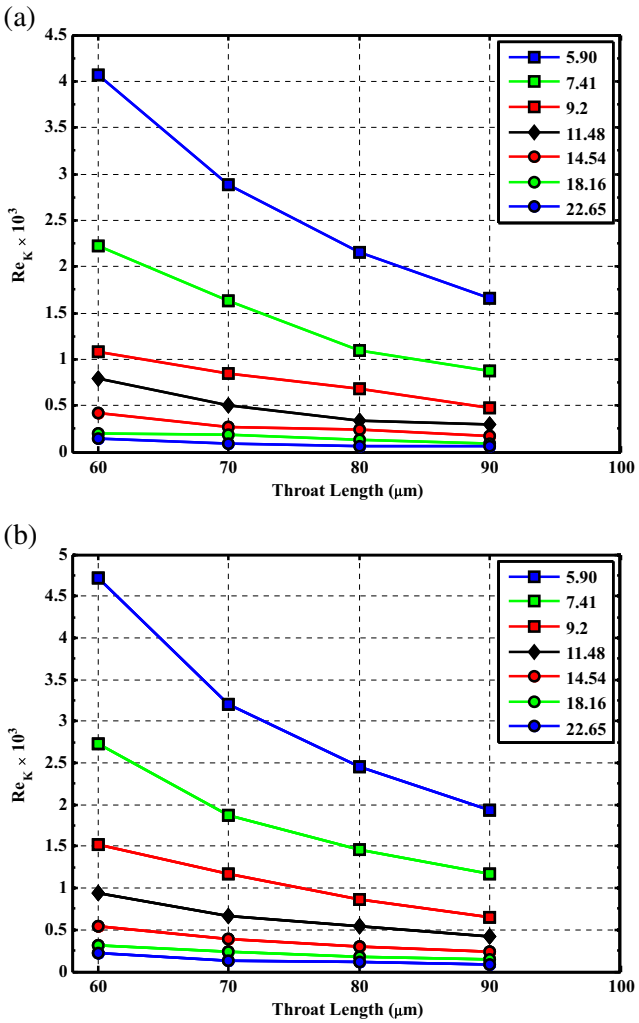

Fig. 18 Permeability Reynolds number versus throat length and average aspect ratio for **a** conical and **b** sinusoidal networks with the average coordination number = 6

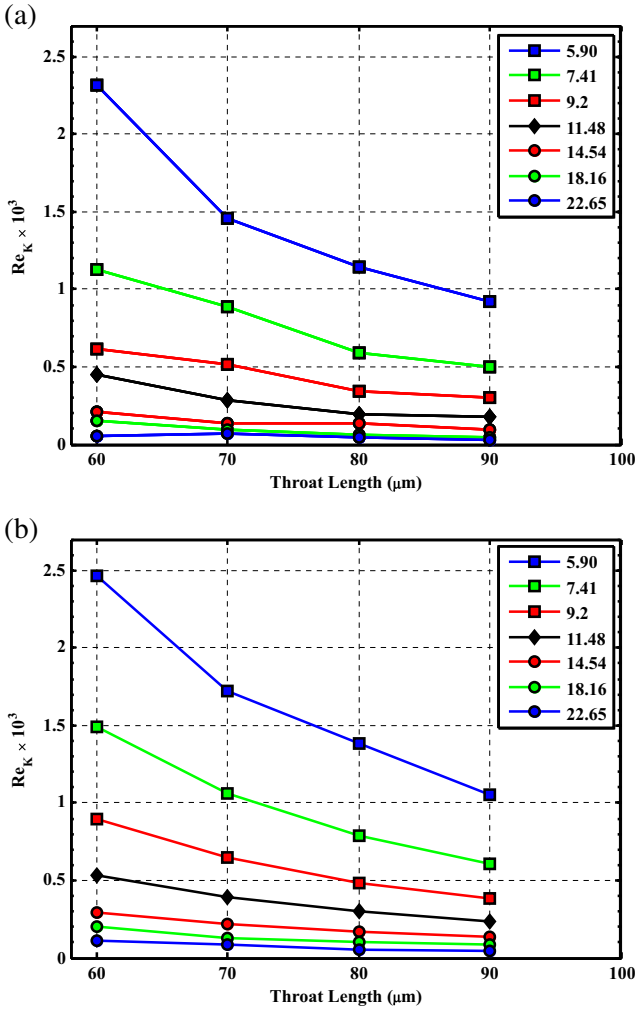

Fig. 19 Permeability Reynolds number versus throat length and average aspect ratio for **a** conical and **b** sinusoidal networks with the average coordination number = 4.5

number. To overcome this problem, applying correlations (proper correlations based on the model are proposed in the next section) for the non-Darcy coefficient can be a promising solution. The critical velocity at which the onset of non-Darcy flow occurs can be determined using Eq. 29.

$$V_C = -1.8830 \times 10^7 \frac{\mu E}{(1-E)K^{-0.2478}\rho}. \tag{29}$$

Since Eq. 29 is correlation based, it is dimensionally inconsistent. In fact, the critical velocity can be re-defined by rearrangement of the Forchheimer equation to eliminate the dependency on the non-Darcy coefficient, as Eq. 30, which shows the critical velocity as a function of the non-Darcy effect (E) and pressure gradient.

$$V_C = \frac{-\frac{dp}{dx}(1-E)K}{\mu}. \tag{30}$$

According to the assumed value of non-Darcy effect (limit of the non-Darcy flow) and total pressure drop along the length of porous media, the critical velocity can be calculated. In Eqs. 29 and 30, permeability (K) is in m^2.

3.3 Correlations

No correlation can relate the dependent variable to the independent one exactly. The correlations presented here are not exceptional. Since the non-Darcy coefficient and tortuosity are the innate properties of each porous media, they must be in relation with the other inherent characteristics of porous media like porosity and permeability. The tortuosity is a measure of flow path deviation from straight line. In microscopic scale, as tortuosity of a porous medium increases, fluid has to pass a longer tortuous path through the medium which results confronting with more resistance

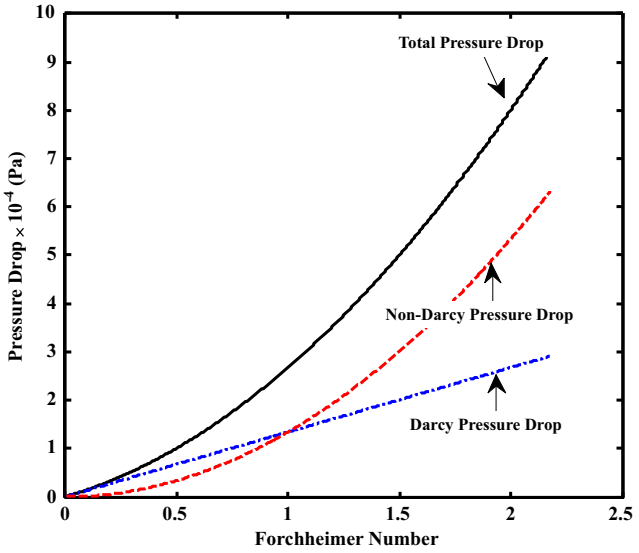

Fig. 20 Darcy, non-Darcy, and total pressure drop as a function of Forchheimer number

against the flow. On the other hand, when a porous medium is more permeable, it provides a less resistance path for flowing of fluid. Thus, in a porous medium, there should be a direct relationship between non-Darcy coefficient and tortuosity and an inverse relationship between non-Darcy coefficient and permeability. It is widely accepted in the literature that the non-Darcy coefficient has a direct relation with the tortuosity and an inverse relation with the porosity and permeability; thus, correlations can be achieved by applying this general relation [30, 56–58]

$$\beta = a\tau^b K^{-c}\varphi^{-d}. \tag{31}$$

The coefficient optimization is done by the imperialist competitive algorithm. The general correlation that reveals the value of non-Darcy coefficient as a function of the permeability can be expressed as

$$\beta = 2.8148 \times 10^{11} K^{-1.2478} \tag{32}$$

and the relation which correlates the non-Darcy coefficient to the permeability/porosity is

$$\beta = 6.9051 \times 10^{9} K^{-1.0477}\phi^{-1.5649}. \tag{33}$$

The correlation coefficients for Eqs. 32 and 33 are 0.998058 and 0.998007, respectively. The unit of permeability is *md*, and the non-Darcy coefficient is in m^{-1}.

In order to examine the validity of model predictions, the correlation results are compared with some experimental data presented in Table 2. In this table, samples 1 to 9 are from Geertsma [59], and the other data are reported by Firoozabadi and Katz [60]. Unfortunately, our seeking for a set of experimental data which simultaneously includes the non-Darcy coefficient, permeability, porosity, and tortuosity

Table 2 Natural sample properties presented by Geertsma [59] and Firoozabadi and Katz [60]

Sample	Permeability (*md*)	Porosity	Measured non-Darcy Coefficient (1/*m*)
1	570	0.152	1.1×10^8
2	19.5	0.112	7×10^9
3	1265	0.204	3.6×10^7
4	235	0.135	2×10^8
5	644	0.208	2.5×10^7
6	181	0.184	9.9×10^7
7	313	0.195	6.9×10^7
8	66	0.138	1.5×10^9
9	73	0.242	3.8×10^8
10	2087	0.267	1.03×10^7
11	1158	0.266	2.3×10^7
12	614	0.24	5.1×10^7
13	178	0.201	1.62×10^8
14	248	0.20	1.29×10^7
15	811	0.233	2.4×10^8
16	1232	0.214	1.46×10^7
17	63	0.217	3.44×10^8
18	16	0.183	7.34×10^9
19	1049	0.255	1.13×10^7
20	117	0.211	3.83×10^8
21	40	0.142	1.16×10^9
22	240	0.153	3.07×10^8
23	665	0.255	4.16×10^7

was not successful. In general, a model predicts the experimental data well if the difference between the measured values and the model's predicted values be small and unbiased. Thus, to determine how the predicted data are close to the observed non-Darcy coefficients, the quality plots for Eqs. 32 and 33 are presented in Figs. 21 and 22, respectively. The *R*-squared for the quality plot of Eq. 32 is 0.9289 and for Eq. 33 is 0.8643. According to the obtained coefficients of determination (*R*-squared values), the presence of the porosity in correlations does not necessarily improve the quality of predicted results. Accordingly, in some cases, correlating the flow-related rock properties to the porosity may not be suitable. This is due to that the porosity is the ratio of the void space to the total volume of porous media and is not an indicator of the pore space geometry which mainly affects the flow behavior.

Table 3 includes the information about the comparison between the *R*-squared values for the correlations presented here and other proposed correlations in the literature. According to this table, suggested correlations based on the model show better agreement with the experimental data. This validation with the experimental data for the non-Darcy coefficient is so supportive and provides confidence

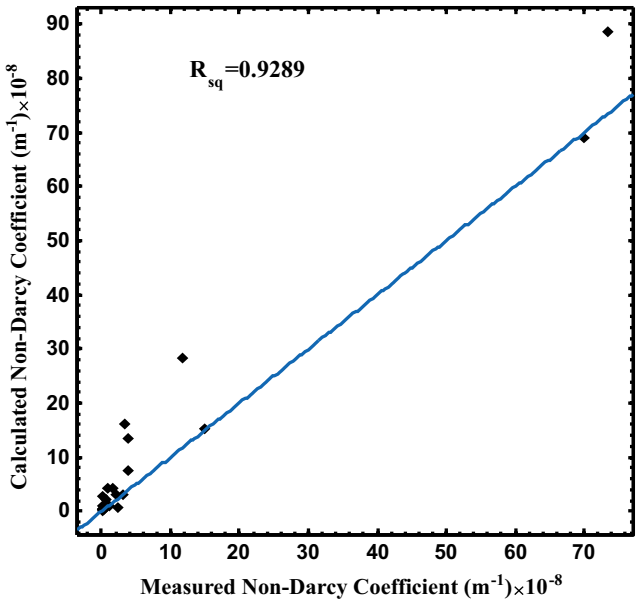

Fig. 21 Quality plot for predicted results by Eq. 32

to utilize the model to predict the tortuosity based on the other inherent properties of porous media. Notwithstanding, the general implementation of model requires more comparisons with some other valid data.

Also, it seems helpful to have some correlations for the value of tortuosity based on the results of the model. As mentioned above, tortuosity as an intrinsic property of porous media is straightforwardly defined as the ratio of the average real passed path to the length of the network in the orientation of applied macroscopic flux. In the case of flow through the soft porous materials, awareness of the value of

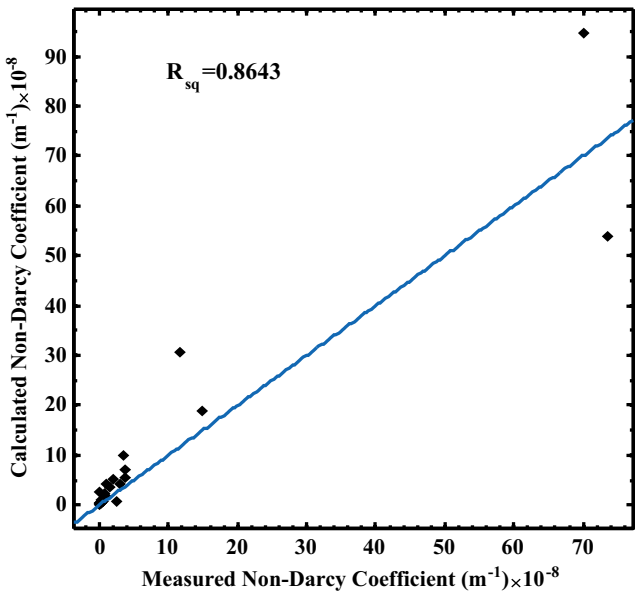

Fig. 22 Quality plot for predicted results by Eq. 33

Table 3 Comparison between R-squared of predicted results of various correlations and experimental data

Model	Correlation	R-squared
Equation 32	$\beta = 2.8148 \times 10^{11} K^{-1.2478}$	0.9289
Equation 33	$\beta = 6.9051 \times 10^{9} K^{-1.0477} \phi^{-1.5649}$	0.8643
Thauvin and Mohanty [30]	$\beta = 2.5 \times 10^{10} K^{-1}$	−17.93
Jones [56]	$\beta = 2.0172 \times 10^{11} K^{-1.55}$	−3.635
Geertsma [59]	$\beta = 1.5915 \times 10^{5} K^{-0.5} \phi^{-5.5}$	−0.3754
Janicek and Katz [57]	$\beta = 1.82 \times 10^{10} K^{-1.25} \phi^{-0.75}$	−5.194
Coles and Hartman [58]	$\beta = 8.1672 \times 10^{11} K^{-1.79} \phi^{-0.54}$	0.7317

tortuosity becomes important as the flow can cause a strain on the matrix and impacts its permeability [61].

Our analysis shows that tortuosity of the network model changes approximately of 5% by changing the average aspect ratio from 5.9 to 22.65, while a variation of the average coordination number from 6 to 4.6 causes a 21% increase in tortuosity. Figure 23 illustrates the relation between the tortuosity and average coordination number of porous media which is the main parameter affecting the tortuosity. On the basis of this data, the correlation between the tortuosity and average coordination number is presented in Eq. 34.

$$\tau = -0.793 \ln(1.011 Cn) + 2.770 \tag{34}$$

where Cn is the average coordination number of the system. The value of coordination number is usually unavailable; hence, a correlation between the tortuosity and other

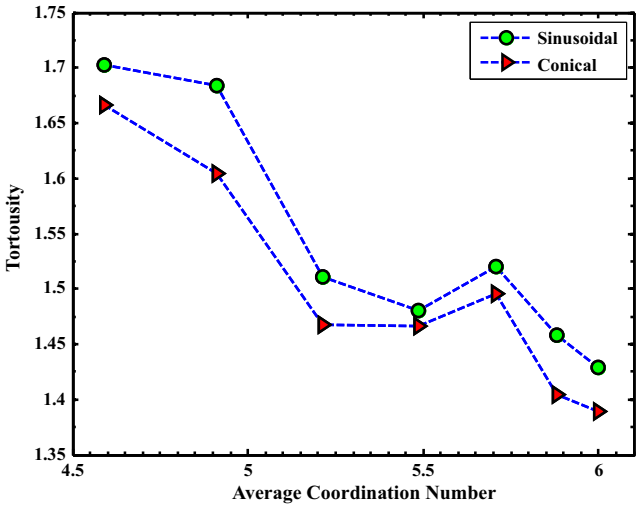

Fig. 23 Relation between average coordination number and tortuosity obtained from network modeling

macroscopic properties of porous media is required. Such correlations are given as follows:

$$\tau = -0.372 \ln(0.134K) + 2.981 \quad (35)$$

where K is in *md* and

$$\tau = 0.235 \ln(0.448\beta) - 2.858. \quad (36)$$

The correlation coefficients of Eqs. 35 and 36 are 0.92 and 0.91, respectively.

4 Conclusions

This study brings some advances in the area of pore network modeling, where the role of more realistic pore geometry on the onset of non-Darcy flow is not well incorporated. Analytical solutions of the one-dimensional Navier-Stokes equations are used to calculate the pressure drop/volumetric flow rate responses along the conical as well as sinusoidal converging/diverging capillary tubes. Suitable pore and throat size distributions are obtained when the fixed parameters of $\sigma = 0.8$ and $\eta = 1.6$ are used in the Weibull distribution function. A detailed sensitivity analysis of various metrics of pore topology characteristics on the permeability and onset of non-Darcy flow as well as new correlations for predicting the tortuosity and non-Darcy coefficient of the medium are presented. Based on the results obtained here, the following conclusions can be drawn:

- Results of this work enable us to estimate the critical Reynolds number at which the onset of non-Darcy flow commences based on the pore geometrical parameters including throat length, average coordination number, and average throat aspect ratio of the porous media.
- New criteria for the onset of non-Darcy flow behavior are presented. The Reynolds number is not sufficient for predicting the onset of inertial flow and some estimations of the pore space geometry are required to provide a more reliable prediction.
- The analysis of flow in single pores with the conical and sinusoidal profiles revealed that there are two different regions for the flow coefficient ratio as a function of the aspect ratio. In one region, an increase in the aspect ratio drastically reduces the permeability ratio of sinusoidal to conical throats while in the other region, it stays approximately constant.
- At network scale, the increase of average aspect ratio initially elevates the difference between the permeability of sinusoidal and conical networks. Then, by additional increase in this ratio, each network permeability approaches to the other. In contrast, the increase of aspect ratio causes the more difference between the non-Darcy coefficients of networks.
- The onset of non-Darcy flow is majorly affected by the aspect ratio and coordination number of throats while the role of throat length is negligible.
- The higher non-Darcy coefficient does not necessarily mean the lower values of the critical apparent velocity of non-Darcy flow onset.
- New correlations for predicting the tortuosity of porous media are developed. The availability of the permeability or non-Darcy coefficient data as an input of the proposed correlations makes them attractive for related engineering applications.

Acknowledgments The authors would like to thank the Salehi's graphical group and Amir Hossein Mousavi for their help in providing the graphical figures.

References

1. Forchheimer: Hydrolik. Teubner, Leipzing and Berlin (1914)
2. Ergun, S.: Fluid flow through packed column. Chem. Eng. Prog. **48**(2), 89–94 (1952)
3. Huang, H., Ayoub, J.A.: Applicability of the Forchheimer equation for non-Darcy flow in porous media. SPE J. **13**(01), 112–122 (2008)
4. Chaudhary, K., Cardenas, M.B., Deng, W., Bennett, P.C.: The role of eddies inside pores in the transition from Darcy to Forchheimer flowsGeophysical Research Letters **38**(24) (2011)
5. Ruth, D., Ma, H.: On the derivation of the Forchheimer equation by means of the average theorem. Transp. Porous Medias **7**(3), 225–264 (1992)
6. Whitaker, S.: The Forchheimer equation: a theoretical development. Transp. Porous Media **25**, 27–61 (1996)
7. Barr, D.w.: Turbulent flow through porous media. Ground Water **39**(5), 646–650 (2000)
8. Forchheimer: Wasserbewegung durch Boden. Z. Ver. Dtsch. Ing. **45**(5), 1781–1788 (1901)
9. Fand, R., Kim, B., Lam, A., Phan, R.: Resistance to the flow of fluids through simple and complex porous media whose matrices are composed of randomly packed spheres. J. Fluids Eng. **109**(3), 268–274 (1987)
10. Chaudhary, K., Cardenas, M.B., Deng, W., Bennett, P.C.: Pore geometry effects on intrapore viscous to inertial flows and on effective hydraulic parameters. Water Resour. Res. **49**(2), 1149–1162 (2013)
11. Mei, C., Auriault, J.-L.: The effect of weak inertia on flow through a porous medium. J. Fluid Mech. **222**, 647–663 (1991)
12. Fourar, M., Radilla, G., Lenormand, R., Moyne, C.: On the nonlinear behavior of a laminar single-phase flow through two and three-dimensional porous media. Adv. Water Resour. **27**(6), 669–677 (2004)
13. Balhoff, M., Mixkelić, A., Wheeler, M.F.: Polynomial filtration laws for low Reynolds number flows through porous media. Transp. Porous Medias **81**(1), 35–60 (2010)
14. Dullien, F.A.: Porous media: fluid transport and pore structure. Academic (2012)
15. Chen, Z., Lyons, S.L., Qin, G.: Derivation of the Forchheimer law via homogenization. Transp. Porous Medias **44**(2), 325–335 (2001)
16. Hassanizadeh, S.M., Gray, W.G.: High velocity flow in porous media. Transp. Porous Medias **2**, 521–531 (1987)
17. Balhoff, M.T., Wheeler, M.F.: A predictive pore-scale model for non-Darcy flow in porous media . SPE J. **14**, 579–587 (2009)

18. Ewing, R.E., Lazarov, R.D., Lyons, S.L., Papavassiliou, D.V., Papavassiliou, J., Qin, G.: Numerical well model for non-Darcy flow through isotropic porous media. Computat. Geosci. **3**, 185–204 (1999)
19. Chilton, T.H., Colburn, A.P.: Pressure drop in packed tubes. Ind Engngc. Chem. **23**(8), 913–919 (1931)
20. Tek, M.R.: Development of a generalized Darcy equation. Trans. AIME **210**, 376–377 (1957)
21. Wright, D.E.: Non-linear flow through granular media. J. Hyd. Div. Trans. ASCE **94**, 851 (1968)
22. deVries, J.: Prediction of non-Darcy flow in porous media. J. lrrig. Drain. Div. ASCE IR2 (1979)
23. Green, L.J., Duwez, P.: Fluid flow through porous metals. J. Appl. Mech **18**, 39–45 (1951)
24. Leonormand, R., Touboul, E., Zarcone, C.: Numerical models and experiments on immiscible displacements in porous media. J. Fluid Mech. **189**, 165–187 (1988)
25. Dillard, L.A., Blunt, M.J.: Development of a pore network simulation model to study nonaqueous phase liquid dissolution. Water Resour. Res. **36**(2), 439–454 (2000)
26. Lopez, X., Valvatne, P.H., Blunt, M.J.: Predictive network modeling of single-phase non-Newtonian flow in porous media. J. Colloid. Interf. Sci. **264**(1), 256–265 (2003)
27. Balhoff, M.T., Thompson, K.E.: Modeling the steady flow of yield-stress fluids in packed beds. AIChE J. **50**(12), 3034–3048 (2004)
28. Chaouche, M., Rakotomalala, N., Salin, D., Xu, B., Yorstos, Y.C.: Capillary effects in drainage in heterogeneous porous media. Chem. Engng. Sci. **49**, 2447–2466 (1994)
29. Sahimi, M.: Flow phenomena in rocks: from continuum models to fractals, percolation, cellular automata, and simulated annealing. Rev. Mod. Phys. **65**, 1393–1534 (1993)
30. Thauvin, F., Mohanty, K.K.: Network modeling of non-Darcy flow through porous media. Transp. Porous Media **19**, 19–37 (1998)
31. Wang, X., Thauvin, F., Mohanty, K.K.: Non-Darcy flow through anisotropic porous media. Chem. Eng. Sci. **54**, 1859–1869 (1999)
32. Piri, M., Blunt, M.J.: Three-dimensional mixed-wet random pore-scale network modeling of two- and three-phase flow in porous media. I. Model description. Phys. Rev. E: Stat. Phys., Plasmas, Fluids **71**, 026301 (2005)
33. Stark, K.P.: Fundamentals of transport phenomena in porous media, vol. 2. Elsevier, Amsterdam (1972)
34. Du Plessis, J.P., Masliyah, J.H.: Mathematical modeling of flow through consolidated isotropic porous media. Transp. Porous Media **3**, 145–161 (1988)
35. Ma, H., Ruth, D.W.: The microscopic analysis of high Forchheimer number flow in porous media. Transp. Porous Media **13**, 139–160 (1993)
36. Zeng, Z., Grigg, R.: A criterion for non-Darcy flow in porous media. Transp. Porous Media **63**, 57–69 (2006)
37. Martins, A.A., Laranjeira, P.E., Lopes, J.C.B., Dias, M.M.: Network modeling of flow in a packed bed. AIChE J. **53**(1), 91–107 (2007)
38. Fatt, M.: The network model of porous media. I. Capillary pressure characteristics. Pet. Trans. **207**, 142–164 (1956)
39. Thompson, K.E., Fogler, H.S.: Modelling flow in disordered packed beds from pore-scale fluid mechanics. AIChE J. **43**, 1377–1389 (1997)
40. Krohn, C.E., Thompson, A.H.: Fractal sandstones pores: automated measurements using scanning-electron microscope images. Phys. Rev. B Condens. Matter. **33**, 6366–6374 (1986)
41. Caruso, L., Simmons, G., Wilkens, R.: The physical properties of a set of sandstone—part 1. The samples. Int. J. Rock Mech. Min. Sci. Geomech. Abstr. **22**, 381–392 (1985)
42. Lao, H.-W., Neeman, H.J., Papavassilou, D.V.: A pore network model for the calculation of non-Darcy flow coefficients in fluid flow through porous media. Chem. Eng. Comm. **191**(10), 1285–1322 (2004)
43. Mohanty, K.K., Salter, S.J.: Multiphase flow in porous media: II. pore-level modeling. Paper presented at the Annual Fall Technical Conference of the SPE-AIME, New Orleans
44. Veyskarami, M., Hassani, A.H., Mohammad Hossein Ghazanfari, M.H.: Modeling of non-Darcy flow through anisotropic porous media: role of pore space profiles. Chem. Eng. Sci. **151**, 93–104 (2016)
45. Arns, J.-Y., Robins, V., Sheppard, A.P., Sok, R.M., Pinczewski, W.V., Knackstedt, M.A.: Effect of network topology on relative permeability. Transp. Porous Media **55**(1), 21–46 (2004)
46. Raoof, A., Hassanizadeh, S.M.: A new method for generating pore-network models of porous media. Transp. Porous Media **81**(3), 391–407 (2010)
47. Ioannidis, M., Chatzis, I.: On the geometry and topology of 3D stochastic porous media. J. Colloid Interface Sci. **229**(2), 323–334 (2000)
48. Sok, R.M., Knackstedt, M.A., Sheppard, A.P., Pinczewski, W.V., Lindquist, W., Venkatarangan, A., Paterson, L.: Direct and stochastic generation of network models from tomographic images; effect of topology on residual saturations. Transp. Porous Media **46**(2-3), 345–371 (2002)
49. Vasilyev, L., Raoof, A., Nordbotten, J.M.: Effect of mean network coordination number on dispersivity characteristics. Transport Porous Media (2012)
50. Ioannidis, M., Chatzis, I.: Network modelling of pore structure and transport properties of porous media. Chem. Eng. Sci. **54**, 1859–1869 (1993)
51. Diaz, C.E., Chatzis, I., Dullien, F.A.L.: Simulation of capillary pressure curves using bond correlated site percolation on a simple cubic network. Transp. Porous Med **2**, 215–240 (1987)
52. Sochi, T.: Newtonian flow in converging-diverging capillaries. arXiv:1108.0163v2 (2012)
53. Formaggia, L., Lamponi, D., Quarteroni, A.: One-dimensional models for blood flow in arteries. J. Eng. Math. **47**(3/4), 251–276 (2003)
54. Sochi, T.: Newtonian flow in converging-diverging capillaries. Int. J. Model. Simul. Sci. Comput. **4**(03), 1350011 (2013)
55. Cengel, Y., Cimbala, J.: Fluid mechanics; fundamentals and application. McGraw-Hill, New York (2006)
56. Jones, S.: Using the inertial coefficient, b, to characterize heterogeneity in reservoir rock, SPE Annual Technical Conference and Exhibition (1987). Society of Petroleum Engineers
57. Janicek, J.D., Katz, D.L.V.: Applications of unsteady state gas flow calculations (1955)
58. Coles, M., Hartman, K.: Non-Darcy measurements in dry core and the effect of immobile liquid. In: SPE Gas Technology Symposium (1998). Society of Petroleum Engineers
59. Geertsma, J.: Estimating the coefficient of inertial resistance in fluid flow through porous media. Soc. Pet. Eng. J. **14**(05), 445–450 (1974)
60. Firoozabadi, A., Katz, D.L.: An analysis of high-velocity gas flow through porous media. J. Pet. Technol. **31**(02), 211–216 (1979)
61. Kataja, M., Rybin, A., Timonen, J.: Permeability of highly compressible porous medium. J. Appl. Phys. **72**, 1271 (1992)